J Musculoskelet Neuronal Interact 2014; 14(1):104-110

Original Article

Hylonome

Magnetic resonance imaging of bone and muscle traits at the hip: an *in vivo* precision study

J.D. Johnston[1,2], L. Liao[2], A.T. Dolovich[1,2], D.A. Leswick[3], S.A. Kontulainen[2,4]

[1]Department of Mechanical Engineering, College of Engineering; [2]Division of Biomedical Engineering, College of Engineering; [3]Department of Medical Imaging, College of Medicine; [4]College of Kinesiology; University of Saskatchewan, Saskatoon, SK, Canada

Abstract

Objective: To determine the *in vivo* precision of MRI-based measures of bone and muscle traits at the hip. **Methods:** Left proximal femoral neck and shaft of 14 participants (5M:9F; age:21-68) were scanned 3 times using a 1.5T MRI. Commercial and custom image processing methods were used to derive bone geometry and strength traits at the proximal femoral neck and shaft along with muscle area of various muscle groups at the shaft site. For precision, root mean square coefficients of variation ($CV\%_{rms}$) and standard deviations (SD_{rms}) were calculated. **Results:** At the femoral neck, $CV\%_{rms}$ for area-based bone measures ranged between 1.7-5.0%; $CV\%_{rms}$ for cortical thickness varied from 4.7 to 5.6%; and $CV\%_{rms}$ for bending, torsional and buckling-based strength indices ranged between 4.6-7.1%. At the femoral shaft, $CV\%_{rms}$ for bone area ranged between 1.2-3.0%; $CV\%_{rms}$ for cortical thickness varied from 1.7 to 2.0%; and $CV\%_{rms}$ for bending and buckling-based strength indices ranged between 1.4-3.1%. For muscle area, $CV\%_{rms}$ ranged between 1.3-4.5%. **Conclusions:** MRI-based measures of bone and muscle traits at the proximal femoral neck and shaft demonstrated *in vivo* precision errors <7.1%. MRI is a promising 3D technique for monitoring changes in bone and muscle at the clinically important hip.

Keywords: MRI, Proximal Femur, Bone, Muscle, Precision

Introduction

Osteoporosis, through its association with age-related fractures, is one of the most common causes of longstanding pain, functional impairment, disability and death in older people[1,2]. Hip fracture, in particular, is a serious life-threatening injury with high mortality (10-20%) in the immediate post-injury period[1,2]. Effective prevention and treatment strategies are needed to reduce the risk and economic burden of hip fractures. In addition to targeting reducing falls among the elderly, strategies aiming to optimizing bone strength development during skeletal growth and preventing bone fragility during aging may reduce such burdens[2]. Reliable *in vivo* imaging tools and methods are essential when assessing the efficacy of strategies focused on bone geometry and strength (i.e., bone's ability to resist fracture).

Sideways falls (and related impact) trigger most elderly hip fractures[3]. During impact, the proximal femur experiences excessive bending, axial compression and a degree of torsional loading. These loading conditions are problematic for the narrow neck region[4] which is comprised of an asymmetric thin-walled cortex and trabecular bone. Proximal femoral cortical bone traits, in particular, have been shown to be an indicator of hip fragility[5-7]. Importantly, imaging-based metrics can be used to assess cortical bone traits and estimate bone's ability to resist bending, torsion and compression. These 'bone strength' metrics include: area moment of inertia and section moduli, which are measures of bone bending and torsional resistance; area, which is a measure of compressive (or tensile) resistance; and buckling ratio, which is a measure of compressive resistance to local buckling applicable for thin-walled structures (such as the femoral neck). Imaging can also be used to assess muscle cross-sectional area, a surrogate estimate of muscle force[8-10] strongly correlated to fall-related measures of physical function[11] and hip fracture incidence[12]. As muscle is

The authors have no conflict of interest. Funding Sources: Canadian Institutes of Health Research (CIHR).

Corresponding author: James (J.D.) Johnston, Department of Mechanical Engineering, University of Saskatchewan, 57 Campus Drive, Saskatoon, SK, S7N 5A9, Canada
E-mail: jd.johnston@usask.ca

Edited by: F. Rauch
Accepted 29 November 2013

believed to play a dominant role mediating bone mass, geometry and strength adaptation[13-15], it is important to simultaneously assess both bone and muscle traits when evaluating the efficacy of prevention strategies aiming to reduce the risk of hip fractures (e.g., exercise therapy).

Current *in vivo* imaging tools used to assess bone and muscle traits at the hip suffer inherent limitations. Dual-energy X-ray Absorptiometry (DXA) combined with Hip Structure Analysis (HSA) offers estimates of proximal femoral strength at the narrow neck, intertrochanteric region and femoral shaft, but the technique represents a complex 3-dimensional (3D) structure as a 2-dimensional (2D) projection with strength estimates limited to the imaged orientation and highly sensitive to femur orientation[16]. Due to the 2D nature of DXA, the tool cannot distinguish cortical from trabecular bone and, to estimate strength, requires HSA to incorporate assumptions regarding cortical:trabecular proportions and 3D shape[17]. The tool also does not offer any information regarding muscle cross-sectional area. Quantitative Computed Tomography (QCT) can be used to acquire 3D bone and muscle geometry and estimate bone strength at clinically relevant fracture sites of the proximal femur, but at the expense of high ionizing radiation doses to radiosensitive tissues in the pelvic region (2.5-3 mSv[18]). Magnetic resonance imaging (MRI) —although seeing little usage for osteoporosis or other musculoskeletal disorders— offers multiplanar 3D images of bone and muscle with the added benefit of nonionizing radiation, and has great potential for assessing bone and muscle traits at the fracture-prone hip.

To date, *in vivo* studies evaluating application of MRI for estimating proximal femoral bone geometry and strength have been limited to one appropriately sized precision study[19] and two smaller reports[20,21]. These studies focused primarily on bone geometry (e.g., cortical thickness) and indices of axial and torsion strength. These studies did not offer information regarding highly relevant bending-based measures of bone strength, such as maximum and minimum principal area moments of inertia and section moduli. Further, to our knowledge no studies have assessed MRI's ability to measure muscle area at the upper thigh region.

The objective of this study was to determine the *in vivo* precision of MRI based measures of hip bone geometry and strength, including strength indices for bending, axial compression, torsion and buckling, in conjunction with upper thigh muscle area.

Methods

Participants

We recruited fourteen study participants (5 males and 9 females; ages ranging from 21 to 68 years, mean 30.5 ± standard deviation (SD) 12 years; weights ranging from 54 to 105 kg, mean 72.1 ± 15 kg). Study approval was obtained from the University of Saskatchewan Biomedical Research Ethics Board and informed consent was provided by all participants prior to study involvement.

MR image acquisition

We obtained MRI scans of the left proximal femoral neck regions using a clinical 1.5T scanner (MAGNETOM Avanto, Siemans, Germany) with a 6 channel body array coil positioned over the hip region. Each participant was oriented supine with legs extended and externally rotated 15°. For the femoral neck, a localizer scan using a T1-weighted spin-echo sequence was applied in the oblique coronal and oblique sagittal directions to determine the orientation of the femoral neck axis. A T1-weighted gradient echo volumetric interpolated breath-hold examination (VIBE) sequence (with parameters: TR 12.7 ms, TE 7.14 ms, 3 excitations, 10° flip angle, 0.49×0.49 mm in-plane pixel size, 5 mm slice thickness, ~5 minute scan time, ~10 images) was then applied in a plane perpendicular to the femoral neck axis. This sequence offered a small in-plane pixel size and was similar to previous approaches used to image the proximal femur[19,22]. For the femoral shaft, axial images (relative to the orientation of the participant) of the hip region were obtained using a T1-weighted turbo spin echo (with parameters: TR 616 ms, TE 12 ms, 2 excitations, 180° flip angle, 0.45×0.45 mm in-plane pixel size, 4 mm slice thickness, ~4.5 minute scan time, ~40 images). The image volume started ~2 cm superior to the femoral head and ended ~5 cm inferior to the lesser trochanter. After piloting a range of sequences, this sequence was selected as it offered a small in-plane pixel size, efficient scanning times, and sufficient contrast between bone, muscle and fat. For the precision analysis, each participant was scanned three times with repositioning and a short walk in-between each scan. A single trained technician took all scans. Each individual scan took approximately 15 minutes, including patient preparation, localizer scan, and imaging of the proximal femoral neck and shaft.

MR image analysis

Image processing

For the femoral neck, the cross-sectional image with the narrowest neck region was visually selected for analysis. This image was selected because it represents the weakest location[23] and followed the standard use of more commonly used DXA-based HSA[17]. For the femoral shaft, a transverse image located 20 mm below the inferior edge of the lesser trochanter was selected for analysis[24]. To identify this location, anisotropic MR image volumes were reconstructed into isotropic volumes (e.g., from 0.45×0.45×4 mm to 0.45×0.45×0.45 mm) using cubic interpolation, and the transverse image was selected from the reconstructed image volume.

Segmentation

Bone and muscle at the femoral neck and shaft were semi-automatically segmented (outlined) using commercial segmentation software (Analyze 10: Mayo Foundation, Rochester, MN, USA). The semi-automatic segmentation process consisted of seeded region growing combined with manual correction via an interactive touch-screen tablet (Cintiq 21UX, Wacom, Krefeld, Germany). Region growing was guided by participant-specific threshold values which defined 50% mid-

point intensity values between adjacent tissues (e.g. cortical bone & trabecular bone, muscle & cortical bone, muscle & fat); a method analogous to the Half-Maximum Height Method[25,26]. Participant-specific thresholds were derived using isolated regional analyses of image intensity of subcutaneous fat, muscle, cortical, and trabecular bone, with the average intensity of adjacent tissues defining respective 50% threshold values. A single researcher (LL) performed all segmentations. For segmenting bone, the periosteal and endocortical surfaces of the femoral neck and shaft were outlined to derive bone traits (Figure 1). For segmenting muscle, four groups were distinguished and segmented according to their movement functionalities: hip extensors (gluteus maximus, semitendinosus, long head of the biceps femoris); hip adductors (adductor magnus, adductor longus, adductor brevis, gracilis); hip flexors (rectus femoris, sartorius); and knee extensors (vastus intermedius, vastus medialis, vastus lateralis).

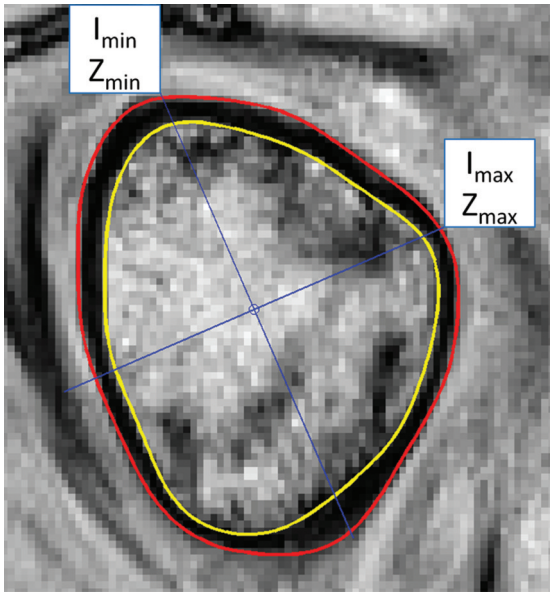

Figure 1. Representative proximal femoral neck segmentation. The black region corresponds to cortical bone, which encloses the trabecular region. The outer red line corresponds to the periosteal surface; inner yellow line corresponds to the endocortical surface. Principal axes used to define bending-based strength indices (principal area moments of inertia I_{max}/I_{min} and section moduli Z_{max}/Z_{min}) are shown in blue and intersect at the cortical bone centroid.

Bone geometry and strength

Following segmentation, custom algorithms (Matlab 2010a; MathWorks, Natick, MA, USA) were used to derive femoral neck and shaft geometrical traits (e.g., cortical wall thickness, periosteal perimeter) and strength indices (e.g., area moments of inertia).

Bone area metrics included: total cross-sectional area (A_{tot}), defined by the area bound by the periosteal surface; trabecular area (A_{trab}), defined by the area bound by the endocortical surface; and cortical area (A_{cor}), defined as the difference between A_{tot} and A_{trab}. At the shaft site, marrow area (A_{marrow}) was calculated in place of trabecular area using the same approach.

Bone perimeter metrics included: periosteal (P_{peri}) and endocortical (P_{endo}) perimeter, defined by the length of smoothed curves fit to the original digitized periosteal and endocortical boundaries. Each smoothed curve was obtained using a smoothing Fourier function (4th order low-pass Butterworth filter)[5].

Mean cortical wall thickness (t) was calculated using two approaches: a circular ring approach (t_c) and an unrolling approach (t_u). The circular ring approach[19] assumes a circular and concentric cortical bone, and calculates mean cortical wall thickness (t_c) by the difference between the outer periosteal radius (r_{peri}) and inner endocortical radius (r_{endo}) using the equation $t_c = r_{peri} - r_{endo} = (P_{peri} - P_{endo})/(2\pi)$. In a circular model, $P_{peri} = 2\pi r_{peri}$ and $P_{endo} = 2\pi r_{endo}$. The unrolling approach treats cortical area as being equal to cortical wall thickness multiplied by the length of the median line running between the periosteal and endocortical edges (defined using $P_{med} = (P_{peri} + P_{endo})/2$). By essentially cutting the segmented area in one location in the axial direction, then unrolling the area, mean cortical wall thickness over the whole region was defined using the equation $t_u = A_{cor}/P_{med}$.

Bending-based strength indices included: principal maximum and minimum area moments of inertia (I_{max}, I_{min}), defined using standard approaches[27,28]; and principal section moduli (Z_{max}, Z_{min}), defined by dividing principal area moments of inertia (I_{max}, I_{min}) by corresponding maximum distances from principal neutral axes to respective outer periosteal edges.

A torsion-based strength index, specifically equivalent polar section modulus (K_{eq}), was defined using Bredt's approach with the formula $K_{eq} = 2(A_{med})t_u$. For this formula, A_{med} refers to the area enclosed by the median line and was defined as the mean of total area and inner trabecular area ($A_{med} = (A_{tot} + A_{trab})/2$), while the unrolling-based mean cortical wall thickness t_u (as opposed to the circular ring-based t_c) was used when calculating K_{eq} as Bredt's equations do not assume a circular and concentric cortical bone. This torsion strength index is applicable for thin walled structures, and was therefore only used at the femoral neck site.

Buckling-based strength indices were determined using two methods: the classic buckling ratio (BR_c), defined by the ratio of maximum outer radius to mean cortical thickness (t_u)[29]; and the area-based buckling ratio (BR_a), defined by the ratio of total area to cortical area[19].

Muscle area

Custom algorithms (Matlab 2010a) were used to derive muscle area for each of the four muscle groups, including hip extensors, adductors, flexors and knee extensors. Total muscle area was defined as the sum of individual muscle group areas.

Statistical analysis

According to procedures outlined by Gluer et al.[30], we assessed the short-term *in vivo* precision of each outcome as a percentage using root mean square coefficients of variation ($CV\%_{rms}$). At the

Site	Tissue	Outcome	Mean	SD_{rms}	$CV\%_{rms}$
Femoral Neck	Bone	Periosteal perimeter, mm	96	0.80	0.8
		Endocortical perimeter, mm	87	0.73	0.8
		Total cross-sectional area, mm^2	736	12.4	1.7
		Trabecular area, mm^2	608	10.2	1.7
		Cortical area, mm^2	128	6.4	5.0
		Mean cortical wall thickness, mm			
		- Circular approach	1.5	0.08	5.6
		- Unrolling approach	1.4	0.07	4.7
		Maximum moment of inertia, mm^4	16667	1143	6.9
		Minimum moment of inertia, mm^4	11407	694	6.1
		Maximum section modulus, mm^3	922	66	7.1
		Minimum section modulus, mm^3	735	48	6.5
		Polar section modulus, mm^3	1880	102	5.5
		Buckling ratio			
		- Classic approach	13.4	0.67	5.0
		- Area-based approach	5.8	0.27	4.6
Femoral Shaft	Bone	Periosteal perimeter, mm	89	0.70	0.8
		Endocortical perimeter, mm	49	0.70	1.4
		Total cross-sectional area, mm^2	632	7.8	1.2
		Marrow area, mm^2	198	6.0	3.0
		Cortical area, mm^2	434	7.5	1.7
		Mean cortical wall thickness, mm			
		- Circular approach	6.4	0.13	2.0
		- Unrolling approach	6.3	0.10	1.7
		Maximum moment of inertia, mm^4	34515	1070	3.1
		Minimum moment of inertia, mm^4	24249	690	2.8
		Maximum section modulus, mm^3	2156	61	2.8
		Minimum section modulus, mm^3	1768	35	2.0
		Buckling ratio			
		- Classic approach	2.6	0.07	2.7
		- Area-based approach	1.5	0.02	1.4
	Muscle	Total muscle area, mm^2	14348	180	1.3
		Hip extensor area, mm^2	2830	127	4.5
		Hip adductor area, mm^2	5462	87	1.6
		Hip flexor area, mm^2	1583	28	1.8
		Knee extensor area, mm^2	3838	69	1.8

Table 1. Precision results for MRI-based measures of proximal femoral bone and muscle traits. Femoral neck bone precision results pertain to 14 participants scanned 3 times each (28 degrees of freedom). Femoral shaft bone and muscle precision results pertain to 13 participants scanned 3 times each (26 degrees of freedom). Mean results are reported for each outcome. Precision is reported using root mean square (RMS) standard deviation (SD_{rms}) of difference between 3 measures and RMS coefficients of variation ($CV\%_{rms}$).

neck site, we assessed the precision of bone outcomes from all 14 participants who were scanned 3 times each (a total of 42 scans, 28 degrees of freedom [DOF]). At the shaft site, we had data from 13 participants, scanned 3 times each (26 DOF), for assessing the precision of bone and muscle outcomes (data for 1 participant was lost due to improper data storage). We report mean values for each outcome for comparison with related precision errors. We also assessed short-term precision in absolute terms using root mean square SD (SD_{rms}) of the differences between the 3 measures. Statistical analyses were performed using commercial software (Matlab 2010a and SPSS 18.0; SPSS Inc, Chicago, IL, USA).

Results

At the femoral neck, $CV\%_{rms}$ precision errors for bone area ranged between 1.7% (A_{tot} and A_{trab}) to 5.0% (A_{cor}); perimeter

$CV\%_{rms}$ results were 0.8% (both P_{peri} and P_{endo}); cortical thickness $CV\%_{rms}$ results varied from 4.7% (t_u) to 5.6% (t_c); and $CV\%_{rms}$ for bending, torsional and buckling-based strength indices ranged between 4.6% (BR_a) and 7.1% (Z_{max}) (Table 1). At the femoral shaft, $CV\%_{rms}$ for bone area ranged between 1.2% (A_{tot}) to 3.0% (A_{marrow}); perimeter $CV\%_{rms}$ results varied from 0.8% (P_{peri}) to 1.4% (P_{endo}); cortical thickness $CV\%_{rms}$ results varied from 1.7% (t_u) to 2.0% (t_c); and $CV\%_{rms}$ for bending and buckling-based strength indices ranged from 1.4% (BR_a) to 3.1% (I_{max}) (Table 1). For muscle area, $CV\%_{rms}$ ranged between 1.3% (total muscle area) to 4.5% (hip extensor area) (Table 1).

Discussion

This study determined the *in vivo* precision of MRI-based measures of proximal femoral bone geometry and strength, in addition to proximal femoral muscle area. This study complements existing MRI-based precision studies at the proximal femur[19-21], and offers a comprehensive evaluation of both bone and muscle at the clinically relevant proximal femoral neck and shaft. To our knowledge, this is also the first *in vivo* MRI study to offer intra-rater precision errors for bending-based maximum and minimum (principal) area moments of inertia and section moduli, in addition to muscle cross-sectional area for various thigh muscle groups.

Our precision results for bone area outcomes compare favorably with *in vivo* measurements made using MRI[19,20]. At the femoral neck, total cross-sectional area $CV\%_{rms}$ was 1.7%, which compares with previous findings ranging from 1.4% to 2.7%[19,20]; and cortical area $CV\%_{rms}$ was 5.0%, which appears smaller than previous findings ranging from 8.9% to 11.7%[19,20]. Similar trends were noted when comparing precision results for geometry and strength calculations to the literature[19]. Mean cortical wall thickness $CV\%_{rms}$ results (circular: 5.6%, unrolling: 4.7%) were smaller than previous results ranging from 11-13.2% using the circular approach[19]; similarly, buckling $CV\%_{rms}$ results (area-based: 4.6%, classic: 5.0%) were smaller than previous results ranging from 7.3-9.9% using an inverse of the area-based approach; and Z_{polar} results ($CV\%_{rms}$ 5.5%) were smaller than previous results ranging from 12.5-15.1%[19]. Our small precision errors are likely attributed to the usage of participant-specific thresholds and semi-automatic region-growing segmentation with minimal user correction (via interaction pen) whereas previous studies depended predominantly upon manual segmentation[19,20]. With regards to muscle area, to our knowledge no MRI-based studies have determined precision errors for muscle areas of the thigh. However, our muscle area $CV\%_{rms}$ results (range: 1.3-4.5%) compare with CT-based precision errors ranging from 1.6% to 2.9% for hip and knee extensor muscle area[8,31,32].

Precision errors of direct measures, such as bone or muscle area, were small (average error less than 2.5%). We consider these precision errors to be an overall indicator of consistent image alignment, image selection, and segmentation. Our high precision may be attributed to: 1) meticulous attention to detail by the MR technician with regards to participant placement and image acquisition; 2) usage of participant-specific threshold values and semi-automatic region growing segmentation, which minimized user-error associated with defining muscle and cortical bone boundaries; and 3) usage of reconstructed isotropic image volumes, which allowed repeatable identification of the 20 mm site below the lesser trochanter.

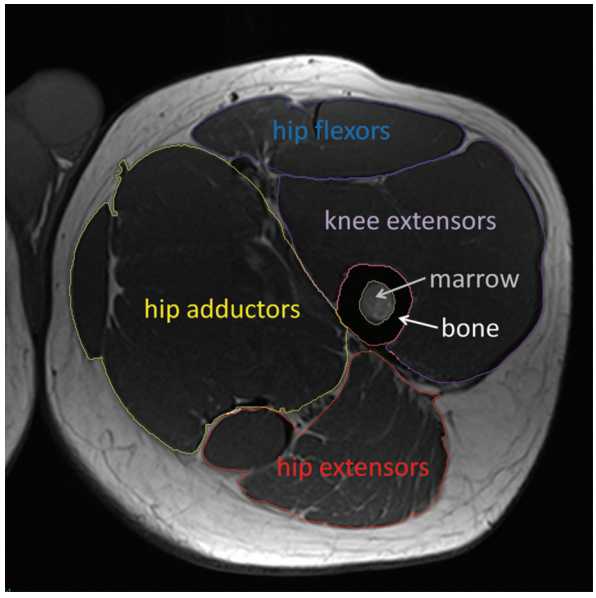

Figure 2. Representative image of proximal femoral shaft bone and muscle segmentations. The black region corresponds to cortical bone, which encloses the marrow region. For the muscle analysis, four groups were distinguished and segmented according to their movement functionalities: hip extensors; hip adductors; hip flexors; and knee extensors. Specific muscles included in the four groups are discussed in the text.

The precision errors of geometrical and strength outcomes which involved mathematical calculations (e.g., cortical thickness, Z_{polar}, BR) appear smaller than previously[19], but higher than direct area measures in this sample. Poorer precision is likely attributed to the combined error of individual precision errors of variables used in the mathematical equations, which increase with each additional variable. As such, outcomes involving minimal calculations with few variables (e.g., simple ratios) should be smaller than those outcomes involving more advanced calculations (e.g., polynomials). It is likely for this reason that precision errors for the unrolling-based cortical thickness and area-based buckling ratio were less than that observed with the ring-based cortical thickness and classic buckling ratio, respectively. Nevertheless, some precision errors of geometrical and strength outcomes involving calculations were >5% (e.g., femoral neck $I_{max,min}$, $Z_{max,min}$). Future studies employing these outcomes will need to assess observed differences (or changes) in relation to precision errors.

Precision errors for cortical wall thickness and buckling

ratio appeared dependent upon the selected analysis approach. Precision errors for cortical wall thickness using the unrolling approach (neck: 4.7%; shaft: 1.7%) appeared to be less than those observed using the circular ring approach (neck: 5.6%; shaft: 2.0%). Variation (SD_{rms}) in measured cortical wall thickness also appeared to be less using the unrolling approach (neck: 0.07 mm; shaft: 0.10 mm) versus the circular approach (neck: 0.08 mm; shaft: 0.13 mm). Given that the circular ring approach offers larger precision errors and variation, and the shape of the bone is not circular but varies with an asymmetrical distribution[5], the unrolling approach should be considered to determine cortical wall thickness. For the buckling ratio, precision errors using the area-based approach (neck: 4.6%; shaft: 1.4%) also appeared to be less than those observed using the classic approach (neck: 5.0%; shaft: 2.7%). As such, the area-based approach may be considered a more precise estimate of cortical rigidity against compressive buckling.

When compared to reported effect sizes in MRI-derived cortical bone traits, observed precision errors appear small. Nikander et al.[22] noted approximately 30% greater femoral neck cortical area and polar section modulus in athletes performing high-impact loading-type exercises (high-jumpers, triple-jumpers) when compared to a non-athletic reference group. Though these results are not directly comparable to this study (due to differences in scanning protocol and analysis methods), they highlight the potential of MRI to capture differences in cortical bone traits at the femoral neck. Prospective follow-ups are needed to assess if observed changes or effects of bone-interventions exceed these precision errors.

This study has certain strengths requiring consideration. First, for the femoral neck analysis we met conservative recommendations for number of subjects and scans by Gluer et al.[30], specifically 28 DOF with 14 subjects and 3 repeated measures. These recommendations are considered sufficient to establish reliable precision errors with an upper 90% confidence limit less than 30%[30]. Although the femoral shaft analysis had a lower number of subjects (n=13), the associated upper 90% confidence limit was ~31%, which did not markedly differ from acceptable intervals proposed by Gluer et al.[30]. Second, we report the precision of bone and muscle outcomes using not only the standard $CV\%_{rms}$ approach, which offers precision as a percentage of the respective metric mean, but also via SD_{rms} which offers precision in absolute terms. Third, we extended mathematical approaches to derive specific bone geometry and strength measures (e.g., cortical thickness and buckling ratio), and reported the precision of each approach. This analysis was useful as it helped us identify which approaches were least affected by accrued precision error. This information has application not only with MRI but also with QCT-based (including peripheral and high resolution QCT) studies of bone geometry and strength.

This study has specific limitations related to subject age and analysis processes. First, the majority of our participants were young adults. This limitation restricts generalizability of these precision errors beyond this age group. A precision study with older individuals is needed for comparison with study findings. Nonetheless, this study was useful to identify 'best case' precision errors within MRI-derived bone and muscle outcomes, which should prove useful when identifying primary and secondary outcome measures in future studies. Second, at the femoral neck it was sometimes difficult to distinguish the boundary between cortical and trabecular bone due to intensity variations in trabecular bone in this transitional zone. Although we defined this boundary using semi-automatic region growing, participant-specific threshold values, and manual correction via a touch-screen pen, in these instances operator experience and judgment played an important part in defining the endocortical surface. Thus, user-error may be a large source of error contributing to poor precision at the femoral neck. Third, it was sometimes difficult to identify the different muscles in corresponding muscle groups due to minimal fat in young participants, resulting in minimal fat:muscle contrast. To account for this we evaluated adjacent inferior and superior images to locate specific muscles, and tracked their location to the site of interest (20 mm below inferior edge of lesser trochanter). However, in some instances uncertainty associated with locating and tracking the muscle groups may partially explain muscle precision errors. Fourth, the femoral neck axis was manually chosen by the MR technician, which likely led to varying femoral shaft images (and associated partial volume effects) from scan to scan. In hindsight, it may have been more appropriate to use a custom fitting technique to locate the neck axis (e.g., axis fit through bisecting lines connecting superior and inferior endocortical surfaces of the femoral neck). Fifth, the smallest femoral neck cross-section was chosen by visual inspection and we are not certain if the selected image corresponded to the weakest location. For future work we aim to analyze adjacent images to quantitatively determine the weakest site. Sixth, the femoral shaft site was selected based upon a fixed 20 mm distance below the inferior edge of the lesser trochanter; a method similar to a previous approach[24]. In future studies, it may be advantageous to select this site based upon a percentage of height or limb length (e.g., 20% of length from center of femoral head to knee joint), particularly if the approach is to be used to longitudinally assess bone traits during growth (e.g., adolescence).

In conclusion, MRI-based measures of bone and muscle traits at the hip demonstrated *in vivo* precision errors <7.1%. This study is among the first to utilize MRI to characterize bone and muscle traits at the proximal femoral neck and shaft. Our results suggest that MRI is a promising 3D technique for monitoring changes in bone and muscle at the clinically important hip.

Acknowledgements

Financial support to conduct the study was provided by the Canadian Institute of Health Research (CIHR) (Grant: MOP98002). SK is a CIHR Regional Partnership Program New Investigator. We thank study participants, Jennifer Layton for guidance regarding MRI sequencing and data acquisition; Nguyen Nguyen for preliminary MATLAB analyses; and Andrew Frank for assistance in study coordination.

References

1. Cummings SR, Melton LJ. Epidemiology and outcomes of osteoporotic fractures. Lancet 2002;359:1761-7.
2. Osteoporosis prevention, diagnosis, and therapy. Jama 2001;285:785-95.
3. Greenspan SL, Myers ER, Kiel DP, Parker RA, Hayes WC, Resnick NM. Fall direction, bone mineral density, and function: risk factors for hip fracture in frail nursing home elderly. The American journal of medicine 1998; 104:539-45.
4. Lovejoy CO. Evolution of human walking. Sci Am 1988;259:118-25.
5. Mayhew PM, Thomas CD, Clement JG, et al. Relation between age, femoral neck cortical stability, and hip fracture risk. Lancet 2005;366:129-35.
6. Crabtree N, Loveridge N, Parker M, et al. Intracapsular hip fracture and the region-specific loss of cortical bone: analysis by peripheral quantitative computed tomography. J Bone Miner Res 2001;16:1318-28.
7. Bell KL, Loveridge N, Power J, et al. Structure of the femoral neck in hip fracture: cortical bone loss in the inferoanterior to superoposterior axis. J Bone Miner Res 1999; 14:111-9.
8. Maughan RJ, Watson JS, Weir J. Strength and cross-sectional area of human skeletal muscle. J Physiol 1983; 338:37-49.
9. Higbie EJ, Cureton KJ, Warren GL 3rd, Prior BM. Effects of concentric and eccentric training on muscle strength, cross-sectional area, and neural activation. J Appl Physiol 1996;81:2173-81.
10. Akima H, Kuno S, Takahashi H, Fukunaga T, Katsuta S. The use of magnetic resonance images to investigate the influence of recruitment on the relationship between torque and cross-sectional area in human muscle. Eur J Appl Physiol 2000;83:475-80.
11. Goodpaster BH, Park SW, Harris TB, et al. The loss of skeletal muscle strength, mass, and quality in older adults: the health, aging and body composition study. J Gerontol A Biol Sci Med Sci 2006;61:1059-64.
12. Lang T, Cauley JA, Tylavsky F, Bauer D, Cummings S, Harris TB. Computed tomographic measurements of thigh muscle cross-sectional area and attenuation coefficient predict hip fracture: the health, aging, and body composition study. J Bone Miner Res 2010;25:513-9.
13. Digirolamo DJ, Kiel DP, Esser KA. Bone and skeletal muscle: neighbors with close ties. J Bone Miner Res 2013;28:1509-18.
14. Burr DB. Muscle strength, bone mass, and age-related bone loss. J Bone Miner Res 1997;12:1547-51.
15. Frost HM. Bone "mass" and the "mechanostat": a proposal. Anat Rec 1987;219:1-9.
16. Beck TJ. Extending DXA beyond bone mineral density: understanding hip structure analysis. Curr Osteoporos Rep 2007;5:49-55.
17. Beck TJ, Looker AC, Ruff CB, Sievanen H, Wahner HW. Structural trends in the aging femoral neck and proximal shaft: analysis of the Third National Health and Nutrition Examination Survey dual-energy X-ray absorptiometry data. J Bone Miner Res 2000;15:2297-304.
18. Engelke K, Adams JE, Armbrecht G, et al. Clinical use of quantitative computed tomography and peripheral quantitative computed tomography in the management of osteoporosis in adults: the 2007 ISCD Official Positions. J Clin Densitom 2008;11:123-62.
19. Sievanen H, Karstila T, Apuli P, Kannus P. Magnetic resonance imaging of the femoral neck cortex. Acta Radiol 2007;48:308-14.
20. McKay HA, Sievanen H, Petit MA, et al. Application of magnetic resonance imaging to evaluation of femoral neck structure in growing girls. J Clin Densitom 2004;7:161-8.
21. Gomberg BR, Saha PK, Wehrli FW. Method for cortical bone structural analysis from magnetic resonance images. Academic radiology 2005;12:1320-32.
22. Nikander R, Kannus P, Dastidar P, et al. Targeted exercises against hip fragility. Osteoporos Int 2009;20:1321-8.
23. Zebaze RM, Jones A, Welsh F, Knackstedt M, Seeman E. Femoral neck shape and the spatial distribution of its mineral mass varies with its size: Clinical and biomechanical implications. Bone 2005;37:243-52.
24. Ito M, Nakamura T, Fukunaga M, Shiraki M, Matsumoto T. Effect of eldecalcitol, an active vitamin D analog, on hip structure and biomechanical properties: 3D assessment by clinical CT. Bone 2011;49:328-34.
25. Kontulainen S, Liu D, Manske S, Jamieson M, Sievanen H, McKay H. Analyzing cortical bone cross-sectional geometry by peripheral QCT: comparison with bone histomorphometry. J Clin Densitom 2007;10:86-92.
26. Spoor CF, Zonneveld FW, Macho GA. Linear measurements of cortical bone and dental enamel by computed tomography: applications and problems. Am J Phys Anthropol 1993;91:469-84.
27. Turner CH, Burr DB. Basic biomechanical measurements of bone: a tutorial. Bone 1993;14:595-608.
28. Martin RB, Atkinson PJ. Age and sex-related changes in the structure and strength of the human femoral shaft. J Biomech 1977;10:223-31.
29. Kim KM, Brown JK, Kim KJ, et al. Differences in femoral neck geometry associated with age and ethnicity. Osteoporos Int 2011;22:2165-74.
30. Glüer CC, Blake G, Lu Y, Blunt BA, Jergas M, Genant HK. Accurate assessment of precision errors: how to measure the reproducibility of bone densitometry techniques. Osteoporos Int 1995;5:262-70.
31. Sipila S, Suominen H. Effects of strength and endurance training on thigh and leg muscle mass and composition in elderly women. J Appl Physiol 1995;78:334-40.
32. Haggmark T, Jansson E, Svane B. Cross-sectional area of the thigh muscle in man measured by computed tomography. Scandinavian journal of clinical and laboratory investigation 1978;38:355-60.